Geophysical Research Letters

RESEARCH LETTER
10.1029/2021GL095683

Key Points:

- An upper bound on magma chamber volume is between 13.6 and 20.6 km^3, depending on trapdoor fault dip (near-vertical faults favored)
- The lower bound on volume is one-half the upper bound
- These volume estimates are inversely proportional to the shear modulus (10 GPa here)

Supporting Information:

Supporting Information may be found in the online version of this article.

Correspondence to:

Y. Zheng,
yjzheng@caltech.edu

Citation:

Zheng, Y., Blackstone, L., & Segall, P. (2022). Constraints on absolute magma chamber volume from geodetic measurements of trapdoor faulting at Sierra Negra volcano, Galapagos. *Geophysical Research Letters*, *49*, e2021GL095683. https://doi.org/10.1029/2021GL095683

Received 5 OCT 2021
Accepted 12 FEB 2022

Constraints on Absolute Magma Chamber Volume From Geodetic Measurements of Trapdoor Faulting at Sierra Negra Volcano, Galapagos

Yujie Zheng[1,2], Laura Blackstone[2], and Paul Segall[2]

[1]Now at Division of Geological and Planetary Sciences, California Institute of Technology, Pasadena, CA, USA, [2]Geophysics Department, Stanford University, Stanford, CA, USA

Abstract Magma chamber volume is critical for volcano hazards assessment and forecasting. Standard geodetic methods constrain volume change, not the total volume. Here, we show that the deformation response of the magma chamber to trapdoor faulting events at Sierra Negra volcano, Galapagos, depends on the product of the absolute chamber volume and the magma compressibility. Bubble-free magma provides the lower limit on compressibility, thus an upper bound on the chamber volume of 13.6–20.6 km^3, depending on fault dip. We estimate an upper limit on compressibility using a conduit model relating volatile content to lava fountain height, compared with observations from the 2005 eruption, constrained by volatile content of olivine melt inclusions. This yields a lower bound on chamber volume roughly half the upper bound. We find that the best fitting trapdoor fault is near-vertical; reverse dips are slightly favored (88°).

Plain Language Summary It is important to understand the size of underground magma reservoirs since the volume of available magma limits the size of short-lived eruptions. In this study, we analyze unique trapdoor faulting events observed at Sierra Negra volcano. These events last only a few seconds and cause distinctive displacements of the ground surface. The volume change and magma pressure drop due to trapdoor faulting depend on the product of chamber volume and magma compressibility. The lower limit of the compressibility is for bubble-free magma. We estimate an upper bound by using observations of "fire fountain" heights during the 2005 eruption of Sierra Negra. Higher gas content, and thus more compressible magma, lead to higher fire fountains. We find an upper bound on the magma volume of 13.6–20.6 km^3, depending on fault dip. We also find that the observed fire fountain height can be fit with plausible H_2O content and up to 0.15 weight % CO_2, which leads to a lower bound of magma volume roughly half the upper bound. Our results will be an important benchmark for comparison with other methods of estimating magma chamber volume and form a useful constraint for other similar volcanoes worldwide.

1. Introduction

The volume of magma reservoirs is critical for volcano monitoring and forecasting. The total volume provides an upper bound on the possible eruptive volume, assuming no recharge during the eruption. Knowledge of subsurface magma volumes also helps constrain models of magma chamber evolution. However, determining the total chamber volume from geophysical methods has been challenging. Seismic tomography can map the distribution of wave speeds and attenuation, but employing these results to estimate volumes of melt is not straightforward (Lees, 2007; Paulatto et al., 2012; Rawlinson et al., 2014). The same is true for electromagnetic imaging. The distribution of earthquake hypocenters can provide a qualitative sense of magma chamber volume, but location uncertainty and the potential for hot, aseismic rock surrounding magma reservoirs limit quantitative analysis. Geochemical mixing models can provide estimates of the volume of the well-mixed portion of shallow reservoirs (D. Geist et al., 2002; D. J. Geist et al., 2005; Pietruszka & Garcia, 1999).

Standard geodetic models constrain the change in chamber volume but place weak if any constraints on total chamber volume (Segall, 2013). This is well expressed, for example, in the "Mogi model" (Mogi, 1958; Yamakawa, 1955), in which the amplitude of surface deformation is proportional to the product of the pressure change Δp and the total volume V, and inversely proportional to the shear modulus, $\Delta pV/\mu$.

The absolute chamber volume can be inferred from geodetic observations if there are independent constraints on pressure change. Such analyses have been conducted at Kīlauea volcano, where surface lava lakes were

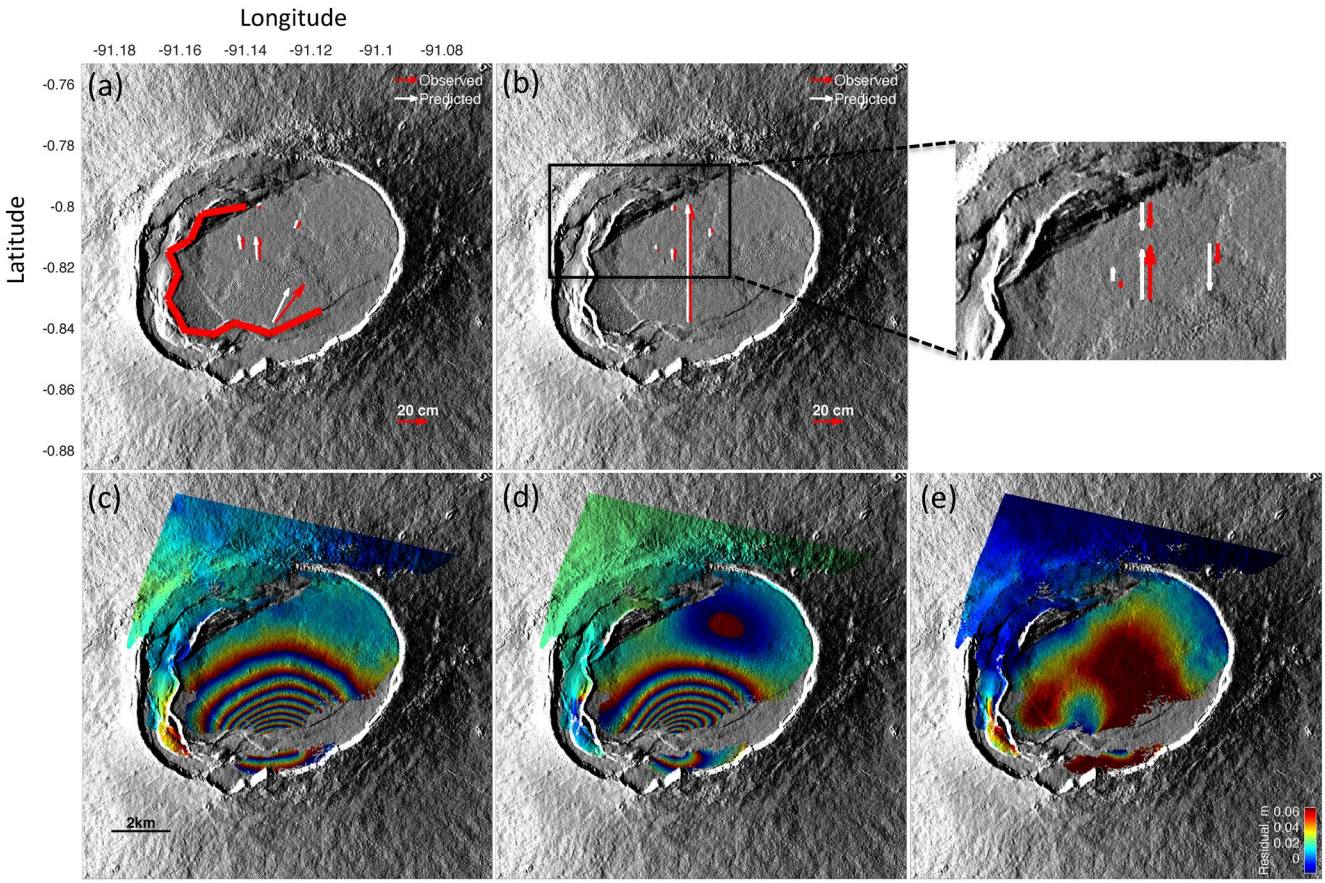

Figure 1. (a) Observed and predicted GPS horizontal displacements from the trapdoor-chamber model shown in Figure 2b of the 16 April 2005 event, overlaid on a shaded relief map of the Sierra Negra Volcano with the intra-caldera fault system shown as thick red lines. (b) Observed and predicted GPS vertical displacements. The inset shows subsidence of the northernmost stations. (c) Observed InSAR data of the 16 April 2005 event re-wrapped at 10 cm fringes. Note that InSAR measurements are discontinuous across the southern fault segments. (d) Predicted InSAR data, re-wrapped at 10 cm fringes. (e) Residuals between observed and predicted InSAR data.

hydraulically connected to the summit chamber, such that changes in lava level can be interpreted as changes in chamber pressure (Anderson et al., 2015; Denlinger, 1997; Johnson, 1992; Segall et al., 2001). Estimates using this approach range from 240 km^3 for the entire magmatic system, including the rift zones (Denlinger, 1997), to 20 km^3 for the summit chamber (Segall et al., 2001), to as low as approximately 1 km^3 for the shallow Halema'uma'u source of episodic deflation-inflation events (Anderson et al., 2015). Most recently, Anderson et al. (2019) combined the remarkable drainage of the summit lava lake during the early stage of Kīlauea's 2018 eruption with Global Positioning System (GPS), tilt, and Interferometric Synthetic Aperture Radar (InSAR) data to constrain the volume of the shallow Halema'uma'u reservoir to between 2.5 and 7.2 km^3 at 68% confidence bounds. In contrast, we show in this work that it is possible to determine the total magma chamber volume from geodetic data even without open conduits from the chamber to the surface. In particular, we show that perturbations in stress associated with trapdoor faulting events allow bounds to be placed on the total volume of the shallow magma chamber at Sierra Negra volcano in the Galapagos, based on the surface deformation response to faulting events.

Sierra Negra is the largest and the most voluminous of the six actively deforming volcanoes in the western Galapagos islands, with the most recent eruption in 2018 (Bell, Hernandez, et al., 2021; Bell, La Femina, et al., 2021; Vasconez et al., 2018). Inflation at Sierra Negra has been punctuated by several trapdoor faulting events, with slip occurring along a complex set of intra-caldera faults with near-vertical scarps (Figure 1a) along the southern and western margins of the caldera (Reynolds et al., 1995). The first indication of trapdoor faulting came from InSAR observations spanning 1997–1998 and is thought to be associated with a M_w 5.0 event on 11 January 1998 (Amelung et al., 2000; Jónsson et al., 2005). A second trapdoor faulting event, associated with a m_b 4.6 earthquake was well captured by both InSAR and GPS data on 16 April 2005 (Chadwick et al., 2006; Jónsson, 2009).

The GPS station GV06 uplifted by almost 1 m within 10 s during this event. In comparison, the prior inflation rate at Sierra Negra was approximately 0.1 cm/day (Chadwick et al., 2006). The short duration implies that negligible amounts of magma left or entered the magma chamber during the faulting event. Both the October 2005 and the June 2018 eruptions were also preceded within hours by trapdoor faulting events (Bell, Hernandez, et al., 2021; Chadwick et al., 2006; Vasconez et al., 2018; S. H. Yun, 2007), suggesting they influenced the timing of the subsequent eruptions.

Here, we analyze both GPS and InSAR data for the trapdoor faulting event on 16 April 2005. We show that the mechanical response of the magma chamber to the trapdoor faulting depends on the product of the total chamber volume and magma compressibility and is clearly expressed in the surface deformation. By constraining the relative compressibility of the magma and the magma chamber it is possible to constrain the absolute volume of the shallow magma reservoir.

2. Method

This section presents a 3D fault-chamber model in an elastic half space to demonstrate the interaction between trapdoor faulting and the magma chamber.We assume that the nearly vertical trapdoor fault system intersects the edges of the horizontal sill-like magma reservoir beneath the caldera. When slip occurs along part of the fault system it forces the edge of the sill adjacent to the fault to open. Before a trapdoor event, magma influx leads to increased pressure and inflationary deformation without fault slip. During the trapdoor event the fault slips while the mass of magma within the chamber remains unchanged. Magma migrates within the reservoir on the time scale of the faulting event to eliminate pressure gradients generated by the sudden fault slip. The combined displacements of the fault and chamber cause nearly instantaneous deformation at the surface that can be measured. As shown below, the fault-induced deformation is dependent on the volume of the magma reservoir and the relative compressibility of the magma and the magma chamber.

Models of deformation at Sierra Negra based on GPS and InSAR data have resolved a sill-like chamber with top at a depth of about 2 km, though a diapir with a flat top also provides an adequate fit (Amelung et al., 2000; Chadwick et al., 2006; S. Yun et al., 2006). We assume that the boundaries of the chamber are uniformly pressurized with no shear traction, consistent with the assumption of nearly static fluid. We use the Displacement Discontinuity Method (DDM) to model a crack-like sill. The boundary conditions on the sill are specified by.

$$\underline{\sigma} = H\underline{\delta} + H_1\underline{s} = -\Delta p\underline{1} \tag{1a}$$

$$\underline{\tau_x} = J_{1x}\underline{s} + J_{2x}\underline{\delta}_x + J_{3x}\underline{\delta}_y = \underline{0} \tag{1b}$$

$$\underline{\tau_y} = J_{1y}\underline{s} + J_{2y}\underline{\delta}_x + J_{3y}\underline{\delta}_y = \underline{0} \tag{1c}$$

where $\underline{\sigma}$, $\underline{\tau_x}$ and $\underline{\tau_y}$ are the normal and horizontal shear tractions in the x and y directions on the sill surface, respectively. $\underline{\delta}$ is the opening of the sill, $\underline{s}$ is a vector of fault slips, and $\underline{\delta}_x$ and $\underline{\delta}_y$ represent shear displacement discontinuities (dislocations) of the sill in the x and y directions. Δp represents perturbation of pressure on the walls of the magma chamber associated with trapdoor faulting, and $\underline{1}$ is a vector of ones. Matrices H and H_1 map displacements into normal stress and matrices J_{ix}, J_{iy}, $i = 1, 2, 3$ map displacements into shear stress; all are computed using results for rectangular and triangular dislocations in a homogeneous elastic half-space (Maerten et al., 2005; Okada, 1992).

Kinematic conditions link the vertical component of slip at the bottom of the fault to opening at the edge of the sill adjacent to the fault.

$$N_z B\underline{s} = E\underline{\delta} \tag{2a}$$

$$N_x B\underline{s} = E\underline{\delta}_x \tag{2b}$$

$$N_y B\underline{s} = E\underline{\delta}_y \tag{2c}$$

where B and E are matrices that extract elements associated with the bottom of the fault and the edge of the sill, respectively. N_z, N_x, and N_y are matrices that extract vertical, east-west, and north-south components of displacements at the bottom of the fault.

The volume change of the magma chamber during a faulting event is found by integrating the opening, $\underline{\delta}$, over the surface of the sill, which can be written compactly as

$$\Delta V = \Psi \Delta p + \Phi \cdot \underline{s} \tag{3}$$

where $\Psi = (dV/dp)_s$ is the volume change per unit pressure change with no slip on the fault and $\Phi \cdot \underline{1}$ is the volume change for unit slip at constant pressure. Ψ is related to the chamber compressibility, $\beta_c = (1/V)\,(dV/dp) = \Psi/V$. Derivations of Ψ and Φ are given in Text S1 in Supporting Information S1. The first term of Equation 3 represents chamber volume change related to stress perturbation caused by trapdoor faulting. The second term gives the direct volume change caused by forced opening at the edge of the sill due to trapdoor faulting.

Since the trapdoor faulting event took place over a few seconds, negligible magma could have entered or exited the chamber. A linearized description of the mass change gives

$$\Delta m/\rho = V \beta_m \Delta p + \Delta V = 0 \tag{4}$$

where ρ and β_m are the magma density and compressibility, respectively.

Equations of mass conservation (Equation 4) and elasticity (Equation 3) provide two independent relations between volume and pressure changes during the faulting event. Combining those yields

$$\Delta p = \frac{-\Phi \cdot \underline{s}}{V \beta_m + \Psi}, \tag{5a}$$

$$\Delta V = \frac{V \beta_m \left(\Phi \cdot \underline{s}\right)}{V \beta_m + \Psi}. \tag{5b}$$

Note that in the limit of small chamber volume and/or incompressible magma, $V\beta_m \to 0$, that $\Delta V \to 0$, while $\Delta p \to -\Phi \cdot \underline{s}/\Psi$. On the other hand in the limit of large volume and/or very compressible magma, $V\beta_m \to \infty$, that $\Delta p \to 0$ and $\Delta V \to \Phi \cdot \underline{s}$. This shows that the volume change of the magma chamber, which can be detected geodetically, is sensitive to the absolute chamber volume and the magma compressibility. Rewriting Equation 5a,

$$V = -\frac{1}{\beta_m}\left(\Psi + \frac{\Phi \cdot \underline{s}}{\Delta p}\right). \tag{6}$$

Note that $\Delta p \leq 0$ (from Equation 5a) and the term in parentheses in Equation 6 is negative, such that $V > 0$.

The surface displacements $\underline{u}$ resulting from the fault-chamber interaction can also be expressed in terms of the vector of slips along the trapdoor fault $\underline{s}$, and a scalar pressure change in the magma chamber Δp,

$$\underline{u} = G_p \Delta p + G_s \underline{s}, \tag{7}$$

where G_p and G_s are computed from rectangular and triangular elastic dislocations. Estimates of Δp and $\underline{s}$ from geodetic measurements, obtained by inverting Equation 7, can be used in Equation 6 together with Ψ and Φ, which are determined by elasticity calculations given the fault and chamber geometry (Equations 4 and 5 in Supporting Information S1). Thus, with bounds on the magma compressibility, β_m, we can bound the absolute magma chamber volume V.

3. Results

We use GPS and InSAR data (from Jónsson, 2009) to estimate the fault slip (assuming pure dip-slip) and pressure change in the magma chamber using Equation 7. The InSAR data has been corrected for inflation during the time span of the SAR acquisitions, both before and after the trap-door faulting (Jónsson et al., 2002). To avoid over-fitting, we smooth the solution by minimizing the second derivative of the fault slip. Specifically we minimize the objective function:

$$F\left(\Delta p, \underline{s}\right) = \left(\underline{u}_{insar} - \underline{\hat{u}}_{insar}\right)^T \Sigma_{insar}^{-1} \left(\underline{u}_{insar} - \underline{\hat{u}}_{insar}\right) + w^2 \left(\underline{u}_{gps} - \underline{\hat{u}}_{gps}\right)^T \Sigma_{gps}^{-1} \left(\underline{u}_{gps} - \underline{\hat{u}}_{gps}\right) + \alpha^2 \|L\underline{\hat{s}}\|_2^2, \quad (8)$$

where $\underline{\hat{u}}$ is the predicted data, L is the second derivative operator, Σ_{insar} and Σ_{gps} are covariance matrices of InSAR and GPS data, respectively. We use data from the nondeforming areas north of the caldera to construct an empirical isotropic covariance matrix Σ_{insar} (Figure S1 in Supporting Information S1). Correlation between GPS measurements are assumed to only exist between horizontal components at a given station. The choice of the smoothness parameter α^2 is based on an "L-curve" (Figure S2 in Supporting Information S1). We weight the GPS data by w^2 to account for the disparity between the number of GPS data points and the number of InSAR data points. We chose a weight factor of $w = 5$ so that fits to both GPS and InSAR data are satisfactory (Figure S3 in Supporting Information S1). We assume a shear modulus of $\mu = 10$ GPa and Poisson's ratio $\nu = 0.25$.

Previous inversions have well constrained the location and the horizontal extent of the chamber during inflationary episodes. We fix the sill geometry as described in S. Yun et al. (2006). To determine the fault dip, we tested a range of dips from outward dipping 70° to inward dipping 70°, constraining the bottom edge of the fault to be aligned with the edge of the sill. The misfit as a function of dip (Figure 2a) is discontinuous because varying the dip changes the projection of the surface expression of the fault. We find that inward (northward on the southern edge of the trapdoor system) dips of 79°N to 85°S provide reasonable fits to both InSAR and GPS data, with a near-vertical, 88° dip being optimal (Figure 2a). In contrast, Chadwick et al. (2006) and Jónsson (2009) concluded the best-fitting faults are more shallowly inward dipping (71°), although their calculations use a planar fault and do not account for mechanical interaction between the fault system and the magma chamber. The preferred model takes the fault to be inward dipping at 88° and only allows dip-slip on the fault. Figure 2b shows the estimated fault slip and the amount of sill opening or closing. Note that the northern edge of the sill, opposite from the sector of the fault with maximum slip, is predicted to have contracted. The estimated pressure change for the preferred model in the chamber is −0.8 MPa and the estimated moment magnitude is Mw 5.3 from fault slip alone, assuming shear modulus of 10 GPa. In contrast, the body wave magnitude of the 16 April 2005 earthquake is mb 4.6 (National Earthquake Information Center; http://neic.usgs.gov). The discrepancy is possibly caused by aseismic fault slip. It is also likely that the seismic radiation was inefficient due to coupling of slip to the viscous magma. Lower shear stiffness in the caldera floor may also contribute to the discrepancy (Chadwick et al., 2006; Jónsson, 2009).

Figure 1 shows the observed and predicted InSAR and GPS displacements. The preferred model can match both GPS and InSAR data quite well. In particular, the model accounts for the modest subsidence in the northern caldera—opposite from the fault segment with the most slip. Previous studies could not capture the observed subsidence with a model restricted to fault slip and not including the magma reservoir (Chadwick et al., 2006; Jónsson, 2009). In addition, our model can explain most of the horizontal displacements recorded in the GPS data without requiring strike-slip motion on the trapdoor fault. The model slightly overpredicts subsidence in the northern caldera. This may reflect oversimplification of the modeled geometry of the fault system or magma reservoir. It is also possible that the estimated fault slip, which is regularized, is slightly biased and impacted on the fit.

4. Discussion

4.1. Upper Bound on Magma Chamber Volume

The product $V\beta_m$ magma chamber volume times magma compressibility is estimated to be 1.7 m^3/Pa. In comparison, Anderson et al. (2019) estimate this product to be 1.3–5.5 m^3/Pa (95% bounds) from deformation and lava lake drainage during the early phase of the 2018 Kīlauea eruption. Segall and Anderson (2021) model episodic caldera collapse during the caldera forming phase of Kīlauea's 2018 eruption and find a range of 1.4–4.1 m^3/Pa. The estimate for Sierra Negra is consistent with these results, but falls toward the lower end of the range for Kīlauea.

Sierra Negra lavas are tholeiitic basalts. For bubble-free basalt, which represents a lower bound on the compressibility, experimental results of Murase and Mcbirney (1973) yield $\beta_m \approx 10^{-10}$ Pa^{-1}. The thermodynamic model MELTS (Ghiorso & Gualda, 2015; Gualda et al., 2012) yields $\beta_m \approx 5.6 \times 10^{-11}$ Pa^{-1} for bubble-free basalt of Sierra Negra composition, roughly a factor of two less than the experimental value. Unless noted, we refer to the

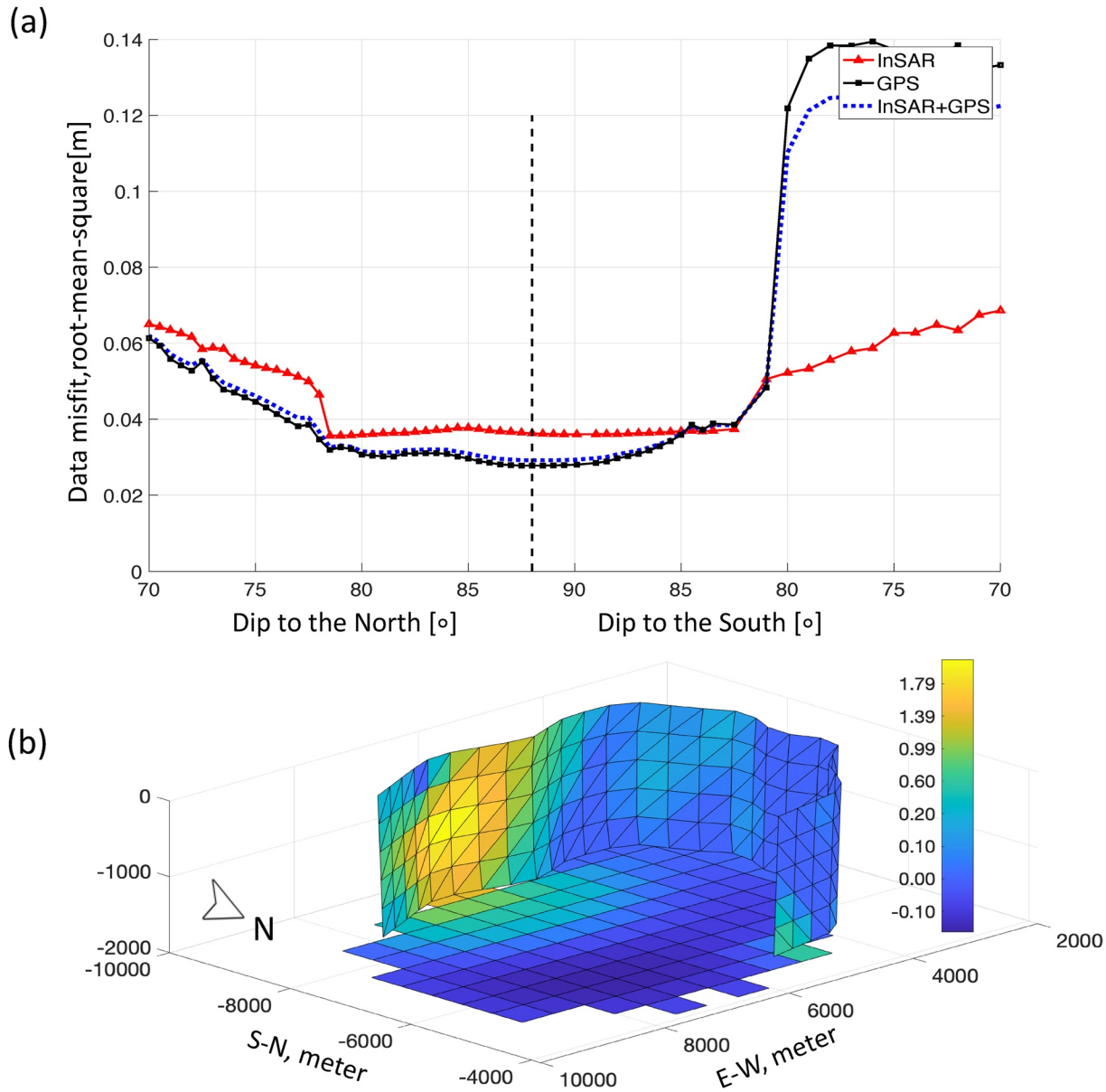

Figure 2. (a) Misfits of GPS (black circles), InSAR (red triangles) and their weighted combination (blue dotted line) as a function of fault dip. The vertical red line shows the optimal fault dip (minimum misfit). (b) Estimated fault slip distribution and sill opening in meters with a 88° inward fault dip. Only dip-slip is allowed on the fault.

experimental value but acknowledge a factor of two uncertainty in this parameter. With the bubble-free experimental value of magma compressibility β_m, we obtain an upper bound on the absolute chamber volume of $V \sim 17.4\ \mathrm{km}^3$, corresponding to a maximum sill thickness of approximately 623 m, given the areal extent of the sill.

Given the high quality of the InSAR and GPS measurements, uncertainties in chamber volume V (Equation 6) mainly stem from uncertainties in the adopted fault-chamber geometry, the choice of elastic constants, and estimated magma compressibility. We address each of these factors in the following.

Inversions of data from previous inflationary episodes have shown that Sierra Negra has a sill-like chamber (Amelung et al., 2000; S. Yun et al., 2006). However, geodetic data is not sensitive to the shape of the chamber as long as the chamber has a flat top. Estimation of the chamber volume V depends on the parameter Ψ (Equation 6), which describes the compressibility of the chamber and is determined by elasticity calculations given the chamber geometry. Perhaps unintuitively, the thickness of the sill has a limited impact on Ψ (the same is

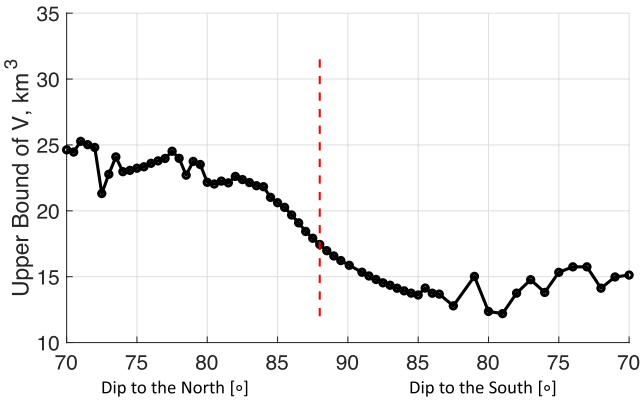

Figure 3. Estimated upper bound of chamber volume as a function of fault dip, assuming a magma compressibility of 10^{-10} Pa^{-1}. The red dashed vertical line indicates the optimal fault dip.

not true for β_c). For a penny-shaped sill at 2 km depth with radius $a = 3$ km in an elastic half-space with $\mu = 10$ GPa, $\Psi = 9.1$ m^3/Pa. In contrast, for a spherical chamber with radius small compared to its depth (the Mogi model) $\Psi \equiv dV/dP = \pi a^3/\mu$. With the same values of a and μ, $\Psi = 8.48$ m^3/Pa, a difference of only 6%. It should be noted that Ψ is inversely proportional to the shear modulus μ. As a result, the estimation of V ($V = \eta\Psi/\beta_m$) is also inversely proportional to μ. Lower values of shear modulus for fractured basalt have been suggested, for example, approximately 3 GPa for Kīlauea (Rubin & Pollard, 1987). Heap et al. (2020) report shear modulus of volcanic rocks with average porosity and fracture density/quality to be 2.1 GPa. These suggest a factor of three to five uncertainty in μ.

Estimation of $\Phi \cdot \underline{s}/\Delta p$, and therefore the estimated reservoir volume, depends on fault dip. Figure 3 illustrates how the estimated upper bound on volume varies with fault dip. Varying the fault dip from 79°S to 85°N, the estimated upper bound of chamber volume ranges from 13.6 to 22.5 km^3. This corresponds to an average thickness ranging from 486 to 805 m and hence the aspect ratio ranging from 0.08 to 0.13.Over this same range of dips, the estimated pressure change within the magma chamber due to trapdoor faulting ranges from −0.81 to −0.93 MPa. The relatively small pressure drop on the chamber is consistent with the observation that the trapdoor faulting event did not significantly perturb the inflation rate (Chadwick et al., 2006, Figure 1d). If the pressure drop had been larger, we might have expected an increase in the inflation rate relative to the prefaulting rate. The trapdoor faulting event immediately before the June 2018 eruption similarly did not significantly impact the uplift rate (Bell, Hernandez, et al., 2021).

4.2. Lower Bound on Magma Chamber Volume

An upper bound on magma compressibility, and hence a lower bound on chamber volume, is obtained by determining the maximum plausible exsolved CO_2 and H_2O volume fraction within the chamber. Following previous studies (Gerlach & Graeber, 1985; Parfitt et al., 1995; Wasser et al., 2021), we use two sets of observations: melt inclusions and observed eruption fountain heights.

Koleszar et al. (2009) analyze olivine melt inclusions from Fernandina lavas similar to those at Sierra Negra. The most volatile-enriched melt inclusions, which are assumed to be representative of primitive mantle-derived magmas, contain up to 6,000 ppm CO_2 and 1.1 wt.% H_2O. More typical samples, assumed to be representative of magma during crustal storage, contain 200–600 ppm CO_2 and 0.5 to 1.1 wt.% H_2O. Peterson et al. (2017) provide compositions for submarine glasses similar in composition and proximity to Sierra Negra with volatile contents ranging from 20 to 188 ppm CO_2 and 0.49 to 1.15 wt.% H_2O. These glasses are thought to be continuously re-equilibrated during ascent, but quenched at sufficient pressure to avoid loss of H_2O.

We use the equilibrate function of MELTS (Ghiorso & Gualda, 2015; Gualda et al., 2012) on a typical Sierra Negra composition from Peterson et al. (2017) with the maximum observed CO_2 content of 6,000 ppm from Koleszar et al. (2009), at pressure and temperature conditions for a chamber 2 km deep. The resulting magma compressibility is approximately 1.5×10^{-9} Pa^{-1} (Figure 4b), a 15-fold increase relative to bubble-free melt. This is an extreme bound on compressibility since some loss of CO_2 from the chamber must occur between eruptions. Taking approximately 600 ppm CO_2 as a more plausible upper bound on CO_2 content within the chamber results in a compressibility of approximately 1.3×10^{-10} Pa^{-1}.

The second approach uses an eruption conduit model to relate volatile content to observed lava-fountain height during the 2005 Sierra Negra eruption (that followed a trap-door faulting event; D. J. Geist et al., 2008). D. J. Geist et al. (2008) report fountain heights of up to 300 m on the second day of the eruption. Days 3–6 saw two primary fountains with heights of 30 and 50 m. On day 7, a single fountain was observed with a height of 50 m. The estimated volume flux at this time was approximately 100 m^3/s from a 6–8 m diameter vent (D. J. Geist et al., 2008). D. J. Geist et al. (2008) employ the Head and Wilson (1987) single vapor phase model to estimate the volatile content on day 7 to be 0.1 to 0.2 weight % water.

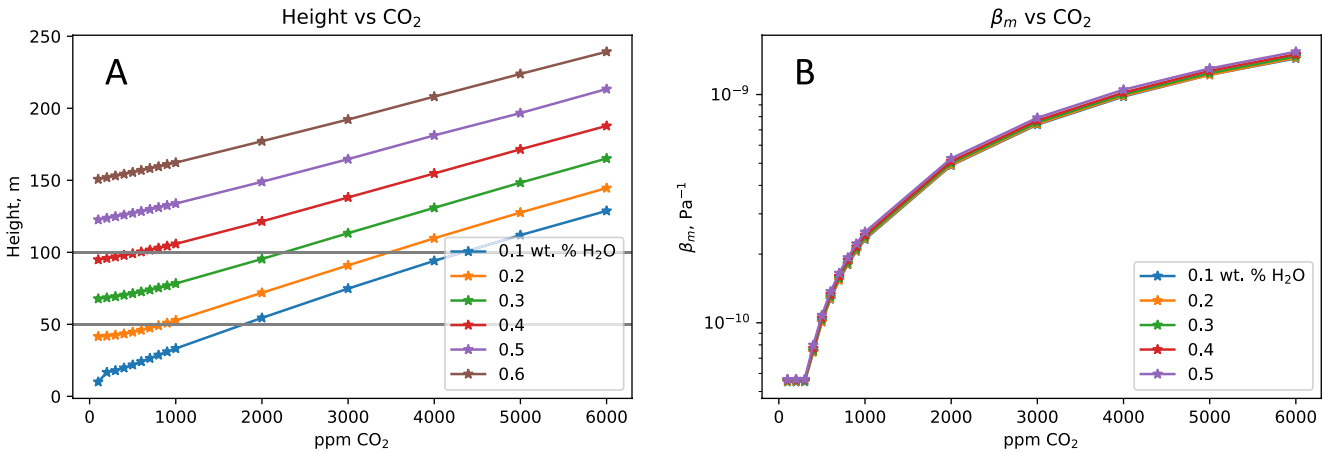

Figure 4. Dependence of fountain height on volatile content. (a) Fountain height as a function of CO_2 content, for various water contents. Horizontal lines mark fountain height of 50 and 100 m. The volume flux is constrained to 100 m^3/s. (b) Magma compressibility β_m within the magma chamber as a function of CO_2 content, for various water contents.

We extend this approach to include both H_2O and CO_2. Specifically, our model assumes a cylindrical conduit, laminar flow up to the magma fragmentation threshold, fixed inlet pressure, and equilibrium H_2O and CO_2 degassing for a Sierra Negra composition derived from MELTS (Ghiorso & Gualda, 2015; Gualda et al., 2012). (Model details and code verification tests are given in Text S1 in Supporting Information S1.)

Parfitt et al. (1995) note that lava ponding, drain back, and bubble coalescence can all decrease the observed height relative to predictions from the Head and Wilson (1987) model. Figures 6a and 6b in Parfitt et al. (1995) shows that for a volume flux of 100 m^3/s, an eruption height of 50 m would be decreased by no more than 50% by these effects. To account for these effects, we estimate volatile compositions that would result in a fountain height of 100 m, twice that observed after the initial phase of the eruption.

Predicted fountain heights depend on both H_2O and CO_2 content, but because water is so much more soluble, the compressibility of magma in the chamber depends primarily on CO_2 content (Figure 4b). Thus, an upper bound on β_m is achieved with a lower value of water content (Figure 4a). A lower bound on water content from Koleszar et al. (2009) and Peterson et al. (2017) is 0.4 wt.%. From Figure 4a, a fountain height of 100 m is obtained with approximately 600 ppm CO_2, which corresponds to a compressibility of approximately 1.3×10^{-10} Pa^{-1}. This is consistent with the estimate based on olivine melt inclusions.

Given that the MELTS-derived compressibility for bubble-free basalt is 5.6×10^{-11} Pa^{-1}, we suggest that a plausible lower bound on magma chamber volume is roughly a factor of two less than the upper bound. It should be noted, however, that the magma chamber may have been stratified with more gas-rich magma toward the top. This could help explain the higher fire fountains observed at the onset of the 2005 eruption (Vigouroux et al., 2008 also noted this possibility).

Thermal considerations presumably also place a lower bound on the magma chamber volume: A very thin sill would likely freeze between recharge events. However, apparently continuous recharge complicates such an analysis, which we defer to future studies.

4.3. An Estimate From Erupted Volume

From the product $V\beta_m$, we can obtain an estimation of the magma-chamber compressibility ratio $\eta \equiv \beta_m/\beta_c = V\beta_m/\Psi$. With a fault dip of 88°N we find $\eta \simeq 0.25$. Alternatively, η can be estimated from the ratio of the erupted volume to the geodetically inferred chamber volume change during the eruption: $\eta = \Delta V_{erupt}/\Delta V - 1$ (Segall, 2010). S. H. Yun (2007) estimates the volume change for the 2005 eruption ΔV to be 0.124 km^3 and the volume of lava that flowed into the caldera ΔV_{erupt} to be 0.141 km^3. D. J. Geist et al. (2008) includes lava outside the caldera and estimates $\Delta V_{erupt} = 0.15$ km^3. Taking the larger value we find $\eta \simeq 0.21\%$, 16% smaller than the estimate based on trapdoor faulting. This change in η reduces the upper bound on chamber volume from 17.4 to

14.6 km^3, for the best-fitting fault dip. Note that this approach provides an independent estimate of the chamber volume as it does not require trapdoor faulting, but simply the erupted and geodetic volume change, as well as magma compressibility.

4.4. Relation to Other Volume Estimates

Body wave tomographic models beneath the Sierra Negra caldera have poor resolution in the shallow crust (less than 3 km depth) and therefore cannot resolve the magma chamber (Tepp et al., 2014). A 3D attenuation model identifies a shallow magma body between 0.5 and 3 km below sea-level (Rodd et al., 2016), which is not inconsistent with our estimate of 623 m sill thickness.

Vigouroux et al. (2008) obtained similar estimates of sill thickness based on analysis of gravity data, however, given the assumptions in their modeling, it is not clear whether this agreement is significant.

5. Conclusions

We have placed bounds on the total volume of the Sierra Negra volcano in the Galapagos by modeling the fault-chamber interaction during the trap-door faulting event on 16 April 2005. Our main findings are:

1. The best-fitting fault that slipped during the 16 April 2005 earthquake is near-vertical and dips steeply inward (reverse slip) at 88°
2. An upper bound on the magma chamber volume is between 13.6 and 22.5 km^3, depending on fault dip. These estimates are for a shear modulus of 10 MPa; V is inversely proportional μ. For the best-fitting dip the volume is 17.4 km^3. The corresponding average sill thickness for the best-fitting dip is 623 m
3. The lower bound on volume is roughly one-half the upper bound
4. These volume estimates are consistent with those obtained from the ratio of the erupted volume to geodetically determined change in magma chamber volume

Finally we note that although our estimations depend on the unique trapdoor faulting system in Sierra Negra there is no obvious reason that the inferred chamber volume would depend on the occurrence of trapdoor faulting. Thus, we expect the estimates presented here to provide useful insights for similar basaltic volcanoes elsewhere.

Data Availability Statement

The InSAR and GPS data used can be downloaded from https://doi.org/10.5281/zenodo.5225160.

Acknowledgments
The research was supported by grants from the National Science Foundation Division of Earth Science (EAR-1829763). The authors would like to thank helpful discussions with Dennis Geist, Mike Stock and others, and thoughtful reviews from William Chadwick and Freysteinn Sigmundsson.

References

Amelung, F., Jónsson, S., Zebker, H., & Segall, P. (2000). Widespread uplift and 'trapdoor' faulting on Galápagos volcanoes observed with radar interferometry. *Nature*, *407*(6807), 993–996. https://doi.org/10.1038/35039604

Anderson, K., Johanson, I. A., Patrick, M. R., Gu, M., Segall, P., Poland, M. P., et al. (2019). Magma reservoir failure and the onset of caldera collapse at Kīlauea Volcano in 2018. *Science*, *366*(6470), eaaz1822. https://doi.org/10.1126/science.aaz1822

Anderson, K., Poland, M., Johnson, J., & Miklius, A. (2015). Episodic deflation–inflation events at Kīlauea volcano and implications for the shallow magma system. *AGU Geophysical Monograph*, *208*, 229–250. https://doi.org/10.1002/9781118872079.ch11

Bell, A. F., Hernandez, S., La Femina, P. C., & Ruiz, M. C. (2021). Uplift and seismicity driven by magmatic inflation at Sierra Negra volcano, Galápagos islands. *Journal of Geophysical Research: Solid Earth*, *126*(7), e2021JB022244. https://doi.org/10.1029/2021jb022244

Bell, A. F., La Femina, P. C., Ruiz, M., Amelung, F., Bagnardi, M., Bean, C. J., et al. (2021). Caldera resurgence during the 2018 eruption of Sierra Negra Volcano, Galápagos islands. *Nature Communications*, *12*(1), 1397. https://doi.org/10.1038/s41467-021-21596-4

Chadwick, W. W., Geist, D. J., Jónsson, S., Poland, M., Johnson, D. J., & Meertens, C. M. (2006). A volcano bursting at the seams: Inflation, faulting, and eruption at Sierra Negra volcano, Galápagos. *Geology*, *34*(12), 1025. https://doi.org/10.1130/G22826A.110.1130/G22826A.1

Denlinger, R. P. (1997). A dynamic balance between magma supply and eruption rate at Kilauea volcano, Hawaii. *Journal of Geophysical Research: Solid Earth*, *102*(B8), 18091–18100. https://doi.org/10.1029/97JB01071

Geist, D., White, W. M., Albarede, F., Harpp, K., Reynolds, R., Blichert-Toft, J., & Kurz, M. D. (2002). Volcanic evolution in the Galápagos: The dissected shield of Volcan Ecuador. *Geochemistry, Geophysics, Geosystems*, *3*(10), 1–32. https://doi.org/10.1029/2002gc000355

Geist, D. J., Harpp, K. S., Naumann, T. R., Poland, M., Chadwick, W. W., Hall, M., & Rader, E. (2008). The 2005 eruption of Sierra Negra Volcano, Galápagos, Ecuador. *Bulletin of Volcanology*, *70*(6), 655–673. https://doi.org/10.1007/s00445-007-0160-3

Geist, D. J., Naumann, T. R., Standish, J. J., Kurz, M. D., Harpp, K. S., White, W. M., & Fornari, D. J. (2005). Wolf volcano, Galápagos archipelago: Melting and magmatic evolution at the margins of a mantle plume. *Journal of Petrology*, *46*(11), 2197–2224. https://doi.org/10.1093/petrology/egi052

Gerlach, T. M., & Graeber, E. J. (1985). Volatile budget of Kilauea volcano. *Nature*, *313*(6000), 273–277. https://doi.org/10.1038/313273a0

Ghiorso, M. S., & Gualda, G. A. R. (2015). An H_2O–CO_2 mixed fluid saturation model compatible with rhyolite-MELTS. *Contributions to Mineralogy and Petrology*, *169*(6), 53. https://doi.org/10.1007/s00410-015-1141-8

Gualda, G. A. R., Ghiorso, M. S., Lemons, R. V., & Carley, T. L. (2012). Rhyolite-MELTS: A modified calibration of MELTS optimized for silica-rich, fluid-bearing magmatic systems. *Journal of Petrology*, *53*(5), 875–890. https://doi.org/10.1093/petrology/egr080

Head, J. W., & Wilson, L. (1987). Lava fountain heights at Pu'u 'O'o, Kilauea, Hawaii: Indicators of amount and variations of exsolved magma volatiles. *Journal of Geophysical Research: Solid Earth*, *92*(B13), 13715–13719. https://doi.org/10.1029/jb092ib13p13715

Heap, M. J., Villeneuve, M., Albino, F., Farquharson, J. I., Brothelande, E., Amelung, F., et al. (2020). Towards more realistic values of elastic moduli for volcano modelling. *Journal of Volcanology and Geothermal Research*, *390*, 106684. https://doi.org/10.1016/j.jvolgeores.2019.106684

Johnson, D. J. (1992). Dynamics of magma storage in the summit reservoir of Kilauea Volcano, Hawaii. *Journal of Geophysical Research: Solid Earth*, *97*(B2), 1807–1820. https://doi.org/10.1029/91jb02839

Jónsson, S. (2009). Stress interaction between magma accumulation and trapdoor faulting on Sierra Negra volcano, Galápagos. *Tectonophysics*, *471*(1–2), 36–44. https://doi.org/10.1016/j.tecto.2008.08.005

Jónsson, S., Zebker, H., & Amelung, F. (2005). On trapdoor faulting at Sierra Negra volcano, Galápagos. *Journal of Volcanology and Geothermal Research*, *144*(1–4), 59–71. https://doi.org/10.1016/j.jvolgeores.2004.11.029

Jónsson, S., Zebker, H., Segall, P., & Amelung, F. (2002). Fault slip distribution of the 1999 Mw 7.1 Hector mine, California, earthquake, estimated from satellite radar and GPS measurements. *Bulletin of the Seismological Society of America*, *92*(4), 1377–1389. https://doi.org/10.1785/0120000922

Koleszar, A. M., Saal, A. E., Hauri, E. H., Nagle, A. N., Liang, Y., & Kurz, M. D. (2009). The volatile contents of the Galapagos plume; evidence for H_2O and F open system behavior in melt inclusions. *Earth and Planetary Science Letters*, *287*(3–4), 442–452. https://doi.org/10.1016/j.epsl.2009.08.029. Retrieved from https://ui.adsabs.harvard.edu/abs/2009E&PSL.287..442K/abstract

Lees, J. M. (2007). Seismic tomography of magmatic systems. *Journal of Volcanology and Geothermal Research*, *167*(1), 37–56. https://doi.org/10.1016/j.jvolgeores.2007.06.008

Maerten, F., Resor, P., Pollard, D., & Maerten, L. (2005). Inverting for slip on three-dimensional fault surfaces using angular dislocations. *Bulletin of the Seismological Society of America*, *95*(5), 1654–1665. https://doi.org/10.1785/0120030181

Mogi, K. (1958). Relations between the eruptions of various volcanoes and the deformations of the ground surfaces around them. *Bulletin of the Earthquake Research Institute*, *36*, 99–134. Retrieved from https://ci.nii.ac.jp/naid/10017329458/

Murase, T., & Mcbirney, A. R. (1973). Properties of some common igneous rocks and their melts at high temperatures. *GSA Bulletin* (Vol. *84*, 11, pp. 3563–3592). https://doi.org/10.1130/0016-7606(1973)84<3563:POSCIR>2.0.CO;2

Okada, Y. (1992). Internal deformation due to shear and tensile faults in a half-space. *Bulletin of the Seismological Society of America*, *82*(2), 1018–1040. https://doi.org/10.1785/BSSA0820021018

Parfitt, E. A., Wilson, L., & Neal, C. A. (1995). Factors influencing the height of Hawaiian lava fountains: Implications for the use of fountain height as an indicator of magma gas content. *Bulletin of Volcanology*, *57*(6), 440–450. https://doi.org/10.1007/BF00300988

Paulatto, M., Annen, C., Henstock, T. J., Kiddle, E., Minshull, T. A., Sparks, R. S. J., & Voight, B. (2012). Magma chamber properties from integrated seismic tomography and thermal modeling at Montserrat. *Geochemistry, Geophysics, Geosystems*, *13*(1). https://doi.org/10.1029/2011gc003892

Peterson, M. E., Saal, A. E., Kurz, M. D., Hauri, E. H., Blusztajn, J. S., Harpp, K. S., et al. (2017). Submarine basaltic glasses from the Galapagos archipelago: Determining the volatile budget of the mantle plume. *Journal of Petrology*, *58*(7), 1419–1450. https://doi.org/10.1093/petrology/egx059

Pietruszka, A. J., & Garcia, M. O. (1999). The size and shape of Kilauea Volcano's summit magma storage reservoir: A geochemical probe. *Earth and Planetary Science Letters*, *167*(3), 311–320. https://doi.org/10.1016/s0012-821x(99)00036-9

Rawlinson, N., Fichtner, A., Sambridge, M., & Young, M. K. (2014). Chapter one - seismic tomography and the assessment of uncertainty. *Advances in Geophysics* In R. Dmowska (Ed.), (Vol. 55, pp. 1–76). Elsevier. https://doi.org/10.1016/bs.agph.2014.08.001

Reynolds, R. W., Geist, D., & Kurz, M. D. (1995). Physical volcanology and structural development of Sierra Negra Volcano, Isabela island, Galápagos archipelago. *GSA Bulletin* (Vol. *107* (12), pp. 1398–1410). https://doi.org/10.1130/0016-7606(1995)107<1398:pvasdo>2.3.co;2

Rodd, R. L., Lees, J. M., & Tepp, G. (2016). Three-dimensional attenuation model of Sierra Negra volcano, Galápagos archipelago. *Geophysical Research Letters*, *43*(12), 6259–6266. https://doi.org/10.1002/2016gl069554

Rubin, A. M., & Pollard, D. D. (1987). Origins of blade-like dikes in volcanic rift zones. *U. S. Geological Survey Professional Paper*, *1350*(2), 1449–1470. Retrieved from https://collaborate.princeton.edu/en/publications/origins-of-blade-like-dikes-in-volcanic-rift-zones

Segall, P. (2010). *Earthquake and volcano deformation*. Princeton University Press. Retrieved from https://www.degruyter.com/document/doi/10.1515/9781400833856/html

Segall, P. (2013). Volcano deformation and eruption forecasting. *Geological Society, London, Special Publications*, *380*(1), 85–106. https://doi.org/10.1144/sp380.4

Segall, P., & Anderson, K. (2021). Repeating caldera collapse events constrain fault friction at the kilometer scale. *Proceedings of the National Academy of Sciences*, *118*(30), e2101469118. https://doi.org/10.1073/pnas.2101469118

Segall, P., Cervelli, P., Owen, S., Lisowski, M., & Miklius, A. (2001). Constraints on dike propagation from continuous GPS measurements. *Journal of Geophysical Research: Solid Earth*, *106*(B9), 19301–19317. https://doi.org/10.1029/2001jb000229

Tepp, G., Ebinger, C. J., Ruiz, M., & Belachew, M. (2014). Imaging rapidly deforming ocean island volcanoes in the western Galápagos archipelago, Ecuador. *Journal of Geophysical Research: Solid Earth*, *119*(1), 442–463. https://doi.org/10.1002/2013jb010227

Vasconez, F., Ramón, P., Hernandez, S., Hidalgo, S., Bernard, B., Ruiz, M., et al. (2018). The different characteristics of the recent eruptions of Fernandina and Sierra Negra volcanoes (Galápagos, Ecuador). *Volcanica*, *1*(2), 127–133. https://doi.org/10.30909/vol.01.02.127133

Vigouroux, N., Williams-Jones, G., Chadwick, W., Geist, D., Ruiz, A., & Johnson, D. (2008). 4D gravity changes associated with the 2005 eruption of Sierra Negra volcano, Galápagos. *Geophysics*, *73*(6), WA29–WA35. https://doi.org/10.1190/1.2987399

Wasser, V. K., Lopez, T. M., Anderson, K. R., Izbekov, P. E., & Freymueller, J. T. (2021). Multidisciplinary constraints on magma compressibility, the pre-eruptive exsolved volatile fraction, and the H_2O/CO_2 Molar ratio for the 2006 Augustine eruption, Alaska. *Geochemistry, Geophysics, Geosystems*, *22*(9), e2021GC009911. https://doi.org/10.1029/2021gc009911

Yamakawa, N. (1955). On the strain produced in a semi-infinite elastic solid by an interior source of stress. *Journal of the Seismological Society of Japan, Ser*, *2*(82), 84–98. https://doi.org/10.4294/zisin1948.8.2_84 Retrieved from https://ci.nii.ac.jp/naid/20001343438/

Yun, S., Segall, P., & Zebker, H. (2006). Constraints on magma chamber geometry at Sierra Negra volcano, Galápagos islands, based on InSAR observations. *Journal of Volcanology and Geothermal Research*, *150*(1–3), 232–243. https://doi.org/10.1016/j.jvolgeores.2005.07.009

Yun, S.-H. (2007). *A mechanical model of the large-deformation 2005 Sierra Negra volcanic eruption from InSAR*. Stanford University.

Reference From the Supporitng Information

Mastin, L. (1995). *A numerical program for steady-state flow of Hawaiian magma-gas mixtures through vertical eruptive conduits (USGS Numbered Series No. 95-756)*. U.S. Geological Survey. Retrieved from http://pubs.er.usgs.gov/publication/ofr95756